

Quadruple and Quintuple Perovskite-Layered Cuprates ($\text{NdDyBa}_{2-x}\text{Sr}_x\text{Cu}_{2+y}\text{Ti}_{2-y}\text{O}_{11-\delta}$ and $\text{NdDyCaBa}_{2-x}\text{Sr}_x\text{Cu}_{2+y}\text{Ti}_{3-y}\text{O}_{14-\delta}$): Their Defect Chemistry and Electrical Properties

N. Mansourian-Hadavi,* D. Ko,† T. O. Mason,*¹ and K. R. Poeppelmeier†

*Materials Science and Engineering Department, Northwestern University, 2225 N. Campus Drive, Evanston, Illinois 60208-3108; and

†Department of Chemistry, Northwestern University, Evanston, Illinois, 60208-3113

Received June 8, 2000; in revised form August 8, 2000; accepted August 15, 2000

DEDICATED TO PROFESSOR J. M. HONIG

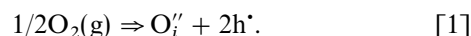
The structure–property relationships of chemically substituted quadruple- and quintuple-layered cuprate perovskites, $\text{NdDyBa}_{2-x}\text{Sr}_x\text{Cu}_{2+y}\text{Ti}_{2-y}\text{O}_{11-\delta}$ and $\text{NdDyCaBa}_{2-x}\text{Sr}_x\text{Cu}_{2+y}\text{Ti}_{3-y}\text{O}_{14-\delta}$, have been investigated with an emphasis on high-temperature electrical properties. Cu doping for Ti in both systems, especially the quadruple system, improves their electrical properties; however, substantial compensation by oxygen vacancies occurs. On the other hand, isovalent Sr substitution for Ba in these systems significantly reduces the ionic compensation, i.e., the $[\text{V}_{\text{O}}^{\bullet\bullet}]$ concentration, as evidenced by thermogravimetry and electrical measurements. Sr substitution not only reduces the Cu–O bond length in favor of hole formation but also introduces metallic behavior as evidenced by *in situ* high-temperature (800–400°C) electrical conductivity and Seebeck coefficient measurements plus low-temperature resistivity measurements. A master plot of high-temperature Seebeck coefficient vs hole content of known superconductors shows that the hole content necessary for superconductivity has been achieved in some of the doped quadruple systems, yet they fail to exhibit superconductivity owing to other structural limitations. © 2000 Academic Press

INTRODUCTION

Quadruple- and quintuple-layered perovskite cuprates have structural characteristics similar to those of known superconductors. All of these materials contain the requisite copper–oxygen two-dimensional sheets interleaved by insulating perovskite blocks, yet they do not superconduct. Quadruple perovskites have two, whereas quintuple perovskites have three blocking layers, interleaved by two CuO_2^{2-} sheets (Fig. 1). Previous work on quadruple and quintuple perovskites has provided a great deal of information about the effects of A and B cation sizes, layering, cation substitu-

tion, and defect chemistry on the physical properties of these materials (1–13). These layered cuprate perovskites form extensive solid solutions with both isovalent and aliovalent substituents, thereby offering the opportunity to investigate a wide range of compositional and structural variations. The present investigation of quadruple ($\text{NdDyBa}_{2-x}\text{Sr}_x\text{Cu}_{2+y}\text{Ti}_{2-y}\text{O}_{11-\delta}$) and quintuple ($\text{NdDyCaBa}_{2-x}\text{Sr}_x\text{Cu}_{2+y}\text{Ti}_{3-y}\text{O}_{14-\delta}$) perovskites was undertaken based upon promising properties (bond lengths, conductivity, and thermopower) in prior work (8).

A small spacing between two adjacent CuO_2^{2-} sheets is crucial for keeping oxygen interstitials out of the intervening space (14). The formation of oxygen interstitials destroys the structural integrity essential to cuprate superconductors and thus is detrimental to superconductivity (15), although it increases hole concentration as shown below:



Therefore, various combinations of A cations (large–large, small–small, and large–small) have been examined to achieve this structural goal (16, 17). It was shown that the use of a large–small rare earth cation combination (e.g., Nd and Dy) can achieve the exclusion of oxygen interstitials between CuO_2^{2-} sheets in layered cuprates (14). The smaller rare earth cation prefers to occupy the 8-coordinate (A'') site between the adjacent Cu–O planes. This reduces the spacing between Cu–O layers, making oxygen intercalation energetically unfavorable, and limits the amount of oxygen incorporation between adjacent copper–oxygen layers.

An important role of the blocking layers in layered cuprate perovskites is to impart a proper mismatch strain to the conducting layers. The bond-mismatch theory of Goodenough (18, 19) expresses the sensitivity of electronic doping to the in-plane bond length mismatch between Cu–O and the blocking layer. Compressive Cu–O bond mismatch stabilizes holes, whereas electrons are stabilized in systems with

¹To whom correspondence should be addressed. Northwestern University, Material Science and Engineering Department, 2225 North Campus Drive, Evanston, IL 60208. Fax: 847-491-7820. E-mail: t-mason@nwu.edu.

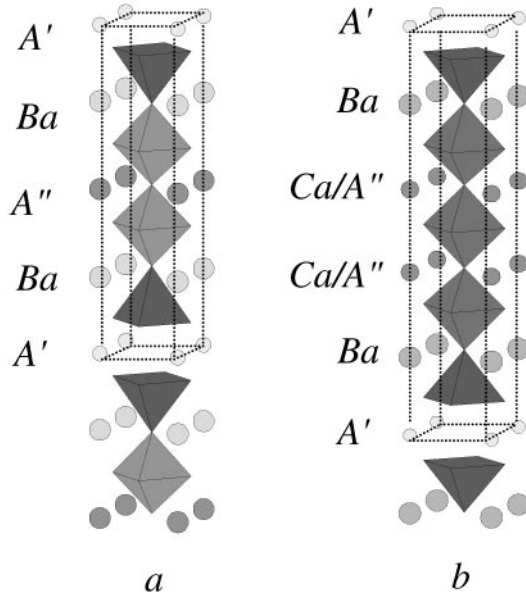


FIG. 1. The polyhedron representation of (a) quadruple and (b) quintuple perovskite-layered cuprates. The blocking layers are lighter and the active layers are darker.

tensile Cu–O bond mismatch. The a -axis lattice parameter is a manifestation of the copper–oxygen in-plane bond length ($a \cong 2(\text{Cu–O})$) and thus is often used as a criterion to determine the nature of bond mismatch. In compressive materials the blocking layer bond lengths ($M\text{–O}$) are smaller than the natural Cu–O in-plane bond length for copper in square pyramidal coordination, thereby imparting a compressive strain in the conducting layers. To relieve the strain in the structure, holes are formed in the active layer (Fig. 2). The vast majority of known high T_c superconductors exhibit this behavior and are p -type (20–26). On the other hand, n -type behavior is observed if the blocking layers ($M\text{–O}$) have bond lengths greater than the natural Cu–O bond length. The resulting tensile strain can stabilize electrons (27). The Cu–O bond lengths for p -type superconductors are about 1.93 Å or less and for n -type superconductors about 1.97 Å or larger (27). If the active and blocking layer bond lengths are similar to each other, there is no driving force for the formation of either holes or electrons. In such cases, aliovalent doping results in ionic point defects (vacancies and interstitials) and few electronic carriers (28, 29).

Quadruple- and quintuple-layered cuprate perovskites with Ti blocking layers have longer Cu–O bond lengths than the known p -type superconductors (compressive structures) but not as long as the known n -type superconductors (tensile structures) (11, 17, 30). In these layered cuprate perovskites, the Ti–O bond lengths are close to the natural Cu–O bond length for copper in square pyramidal coordination. Therefore, there is insufficient compressive or tensile character to favor carrier formation as a strain reliever. Consequently, these materials have a low carrier concentra-

tion and do not superconduct. In this regard, the quintuple perovskites are better prospects, owing to their somewhat shorter Cu–O bond lengths. The present study was undertaken to enhance the transport properties of these layered perovskites and to elucidate their unique defect chemistry.

Electronic or ionic compensation occurs upon aliovalent substitution to satisfy electroneutrality. Electronic compensation is desired for superconductivity since it increases the carrier concentration. For example, in $\text{LaYCaBa}_2\text{Cu}_{2.2}\text{Ti}_{1.8}\text{O}_{14-\delta}$ (5) substitution of Cu^{2+} for Ti^{4+} can conceivably produce two holes, such that the neutrality condition is given by

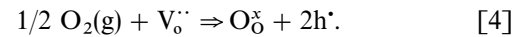
$$2[\text{Cu}_{\text{Ti}}''] = h^{\cdot} \quad [2]$$

Instead, copper doping often results in ionic compensation by the formation of oxygen vacancies:

$$[\text{Cu}_{\text{Ti}}''] = [\text{V}_{\text{O}}^{\cdot\cdot}] \quad [3]$$

It has been suggested that the oxygen vacancies are located in the extreme apices of the top/bottom blocking layer octahedra in the quintuple perovskites (14) where copper preferentially substitutes for titanium (see Fig. 3). Whereas copper can exist in several coordination environments, titanium strongly prefers octahedral coordination, which is preserved if the copper substitutes only into top or bottom layers, with the associated vacancy between it and the adjacent Cu–O layer.

Once formed, these vacancies can be subsequently filled by oxygen, releasing charge carriers according to



Prior efforts to refill these vacancies by different methods have been partially successful (13, 31). This hole generation mechanism is preferred over that of Eq. [1] since deleterious

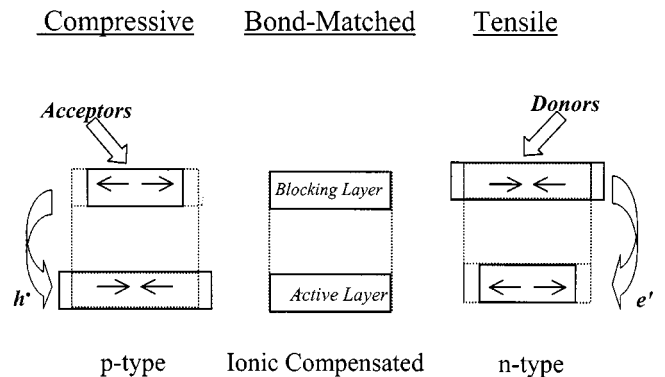


FIG. 2. Schematic summarizing the bond mismatch argument of Goodenough (18). Holes or electrons are injected into the active layer to relieve the mismatch stresses in compressive and tensile structures. The bond-matched systems do not promote creation of carriers (28, 29).

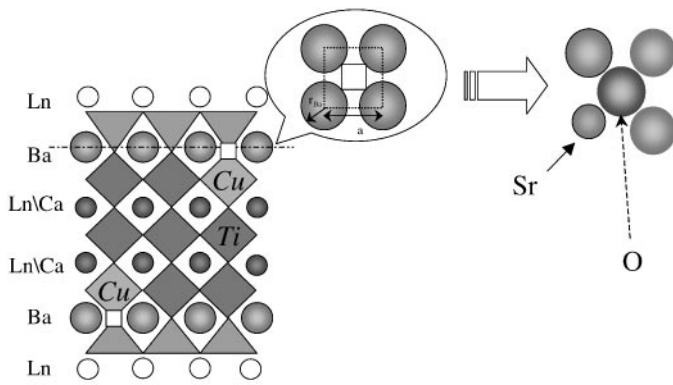


FIG. 3. Schematic view of Sr substitution on the Ba site in the quintuple perovskite structure (differently sized ions) and the oxygen vacancy locations. Vacancies are shown as empty squares.

oxygen interstitials are avoided. Conductivity/thermopower data (for specimens cooled slowly under 1 atm oxygen from 800 to 400°C) showed that partial refilling of those oxygen vacancies is achieved in the $\text{NdDyBa}_{1.5}\text{Sr}_{0.5}\text{Cu}_{2.2}\text{Ti}_{1.8}\text{O}_{11-\delta}$ quadruple system (16). This was thought to be related to the change in oxygen vacancy environments brought about by the strontium co-substitution (5). The smaller size of Sr^{2+} relative to that of Ba^{2+} may provide more space around the oxygen vacancy site, thereby making vacancy refilling easier. Figure 3 illustrates the substitution for Ba in the quadruple perovskite structure.

This work examines the effect of $[\text{Sr}_{\text{Ba}}^x]$ co-substitution on aliovalent doping and oxygen vacancy refilling in both quadruple and quintuple perovskites. In addition, the reduction of in-plane Cu–O bond length as a result of the substitution was also investigated. Simultaneous high-temperature, equilibrium electrical conductivity, and thermopower measurements were made to provide information on both the defect structures and the transport properties of these materials. X-ray powder diffraction, low-temperature resistivity, and magnetic susceptibility measurements were also employed to characterize the samples.

EXPERIMENTAL

Two series of samples were prepared, corresponding to the stoichiometry $\text{NdDyBa}_{2-x}\text{Sr}_x\text{Cu}_{2+y}\text{Ti}_{2-y}\text{O}_{11-\delta}$ (quadruple perovskite) and the stoichiometry $\text{NdDyCaBa}_{2-x}\text{Sr}_x\text{Cu}_{2+y}\text{Ti}_{3-y}\text{O}_{14-\delta}$ (quintuple perovskite). Typically, 4–5 g of samples was prepared by solid state reaction of stoichiometric amounts of Ln_2O_3 ($\text{Ln} = \text{Nd}, \text{Dy}$), ACO_3 ($A = \text{Ba}, \text{Sr}, \text{Ca}$), CuO , and TiO_2 , all of purity above 99.99%, using a Sartorius balance (Brinkmann Instrument, Westbury, NY) with ± 0.1 -mg accuracy. The reagents were ground with mortar and pestle and fired in high-density alumina crucibles at 950°C in air for 1 day to remove carbonates. Each sample was then ground and pressed at ~ 2 MPa into pellets 12.5-mm in diameter and 3- to 5-mm

thick. The pellets were then fired at 1030–1050°C over the course of a 5- to 7-day reaction period, with several intermittent regrindings.

The phase purity of the air-quenched polycrystalline samples was determined by X-ray powder diffraction on a Rigaku diffractometer with Ni-filtered $\text{CuK}\alpha$ radiation. Data were collected from 10° to $80^\circ 2\theta$ with a step size of 0.05° and a collection time of 2 s at each step. Silicon was used as an internal standard. Lattice parameters were determined by pattern matching, Le Bail fitting (32), based on a tetragonal unit cell ($P4/mmm$). The fitting was made with the GSAS program (33).

To determine the oxygen stoichiometry and average copper valence in the samples, hydrogen reduction thermogravimetry was performed (TA Instrument 2950, New Castle, DE). Oxygen annealing of the samples was performed prior to TGA analysis, by equilibrating in flowing oxygen at 900°C and then slowly cooling to room temperature ($< 1^\circ\text{C}/\text{min}$). For TGA runs, samples were preheated at 120°C for 2 h to remove any possible moisture. They were then heated to 900°C at the rate of $5^\circ\text{C}/\text{min}$, isothermally maintained for 10 h and then cooled to room temperature. The whole process was carried out in a 7% H_2/N_2 mixture to achieve the desired reduction.

Simultaneous four-point dc conductivity and Seebeck coefficient measurements, at temperatures from 800 to 650°C, were performed using the technique described previously (34, 35). Rectangular bar-shaped samples ($3 \times 3 \times 9$ mm) were cut from sintered pellets and placed between Au foils, the outer electrodes for electrical measurements, with auxiliary Au wire electrode loops at $\sim 1/3$ and $\sim 2/3$ positions along each bar. A Pt and Pt/Rh thermocouple (type S) was placed in contact with each of the four contacts along the bar. Samples were equilibrated in oxygen partial pressures ranging from 10^{-5} to 1 atm using oxygen or oxygen–argon premixtures. Measurements were taken after equilibrium had been achieved (6–10 h). Conductivity/thermopower data were also taken during slow cooling over the temperature range 800 to 400°C under flowing pure oxygen at a cooling rate of $20^\circ\text{C}/\text{h}$. The measured conductivities were corrected for the porosity of the samples (relative density of 70%) (36).

Low-temperature resistivity measurements were made on select samples, in the range 5–300 K. Measurements were conducted using a standard four-point probe technique on bar-shaped, oxygen-annealed specimens. Electrical contacts were made using silver paint, and measurements were carried out using current densities in the range 0.1–1 mA/cm^2 .

RESULTS AND DISCUSSION

Solid Solution with Strontium

X-ray diffraction experiments detected no impurity phases in the $\text{NdDyBa}_{2-x}\text{Sr}_x\text{Cu}_{2+y}\text{Ti}_{2-y}\text{O}_{11-\delta}$ system for

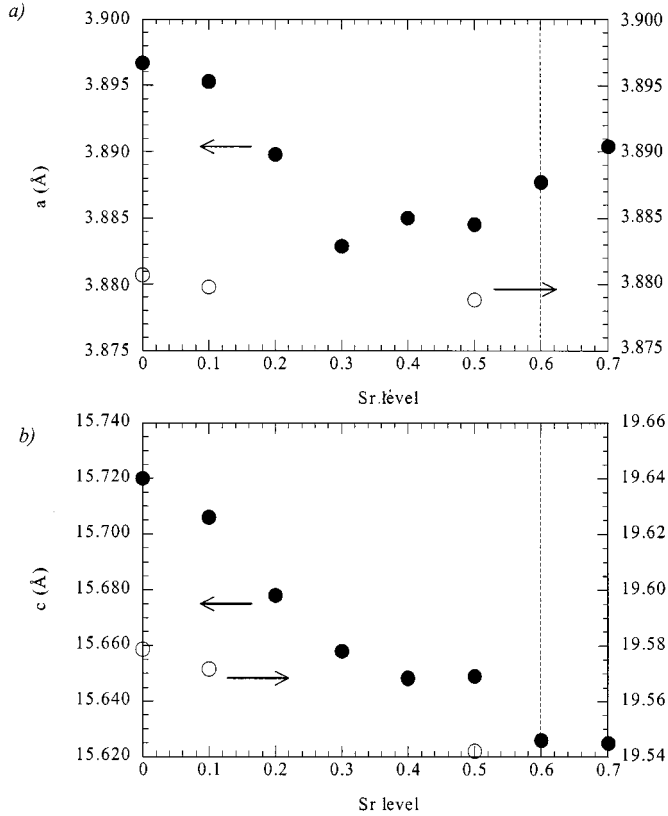


FIG. 4. The variation of lattice parameters as a function of substitution level. (a) a lattice parameter and (b) c lattice parameter of $\text{NdDyBa}_{2-x}\text{Sr}_x\text{Cu}_{2.2}\text{Ti}_{1.8}\text{O}_{11-\delta}$ (filled symbols) and $\text{NdDyCaBa}_{2-x}\text{Sr}_x\text{Cu}_{2.2}\text{Ti}_{2.8}\text{O}_{14-\delta}$ (open symbols). The phase boundary is indicated by the vertical dashed lines.

$0 \leq x \leq 0.6$ and $0 \leq y \leq 0.2$ and in the $\text{NdDyCaBa}_{2-x}\text{Sr}_x\text{Cu}_{2+y}\text{Ti}_{3-y}\text{O}_{14-\delta}$ system for $0.0 \leq x \leq 0.5$ and $0.0 \leq y \leq 0.2$. Samples with higher dopant levels yielded multiphase compounds. Figures 4a and 4b report the a and c lattice parameters of quadruple and quintuple samples as a function of Sr substitution level. Both a and c lattice parameters decrease with Sr substitution, but the shrinkage along the c axis is more pronounced than that along the a axis for both quadruple and quintuple systems. In the quadruple compounds the a -axis shrinkage is steady up to $x = 0.3$ and then levels out (or even relaxes slightly) thereafter. The reduction of the c lattice parameter follows a clearer trend; therefore, it was used to determine the solubility limit, shown by the dashed line in Figs. 4a and 4b. Although the general structural trends of the quintuple system in Figs. 4a and 4b are similar to those of the quadruple system, the extent of shrinkage in response to Sr substitution is much smaller for the quintuple system than for the quadruple counterpart. This could be the result of a much smaller unit layer volume (cell volume divided by the number of perovskite layers, 4 for quadruple or 5 for quintuple) of the

quintuple structure than of the quadruple structure. Consequently, less room will be available for further reduction of cell volume and for oxygen refilling with Sr substitution. Although the a axes for the quintuple systems are shorter than those for the quadruple materials and are closer to the in-plane lattice parameter of known cuprate superconductors, there is apparently insufficient compressive bond mismatch, as evidenced by more severe ionic compensation observed in TGA studies (see below).

Thermogravimetric Results

The oxygen contents of the quadruple and quintuple perovskites for both as-synthesized (air-quenched) and oxygen-annealed samples are summarized in Table 1. If we assume that oxygen interstitials are not present in significant concentration, the oxygen content should be representative of the oxidation state of the Cu–O layers. For example, $\delta = 0.2$ in $\text{NdDyBa}_{2-x}\text{Sr}_x\text{Cu}_{2.2}\text{Ti}_{1.8}\text{O}_{11-\delta}$ and $\text{NdDyCaBa}_{2-x}\text{Sr}_x\text{Cu}_{2.2}\text{Ti}_{2.8}\text{O}_{14-\delta}$ corresponds to strictly divalent copper, which is the result of ionic rather than electronic compensation. The oxygen-annealed sample of $\text{NdDyBa}_{1.5}\text{Sr}_{0.5}\text{Cu}_{2.2}\text{Ti}_{1.8}\text{O}_{11-\delta}$ has higher oxygen content than the air-quenched sample. This suggests that the smaller Sr ion does make oxygen vacancy refilling easier; however, the analogous quintuple sample shows insensitivity to oxygen treatment, presumably owing to the more compact structure. The data in Table 1 show that all the Sr-substituted quadruple samples have higher oxygen and hole (p) contents than those without Sr substitution. Hole concentrations were calculated based on their oxygen contents. These results imply that the Sr substitution effectively introduces hole carriers into the Cu–O conducting planes of these quadruple perovskites. This is corroborated by the

TABLE 1
Oxygen Content of Quadruple and Quintuple Samples from TGA (the Hole Content Was Calculated per One Copper Atom)

Compound	Oxygen content	Hole content	Oxygen-annealed/air-quenched
Quadruple samples			
$\text{NdDyBa}_2\text{Cu}_2\text{Ti}_2\text{O}_{11-\delta}$	11.00 ± 0.02	0.00 ± 0.01	Air-quenched
$\text{NdDyBa}_2\text{Cu}_{2.2}\text{Ti}_{1.8}\text{O}_{11-\delta}$	10.88 ± 0.02	0.06 ± 0.01	Oxygen-annealed
$\text{NdDyBa}_{1.9}\text{Sr}_{0.1}\text{Cu}_{2.2}\text{Ti}_{1.8}\text{O}_{11-\delta}$	10.93 ± 0.02	0.11 ± 0.01	Oxygen-annealed
$\text{NdDyBa}_{1.8}\text{Sr}_{0.2}\text{Cu}_{2.2}\text{Ti}_{1.8}\text{O}_{11-\delta}$	10.91 ± 0.02	0.10 ± 0.01	Oxygen-annealed
$\text{NdDyBa}_{1.7}\text{Sr}_{0.3}\text{Cu}_{2.2}\text{Ti}_{1.8}\text{O}_{11-\delta}$	10.93 ± 0.02	0.12 ± 0.01	Oxygen-annealed
$\text{NdDyBa}_{1.6}\text{Sr}_{0.4}\text{Cu}_{2.2}\text{Ti}_{1.8}\text{O}_{11-\delta}$	10.91 ± 0.02	0.10 ± 0.01	Oxygen-annealed
$\text{NdDyBa}_{1.5}\text{Sr}_{0.5}\text{Cu}_{2.2}\text{Ti}_{1.8}\text{O}_{11-\delta}$	10.93 ± 0.02	0.12 ± 0.01	Oxygen-annealed
$\text{NdDyBa}_{1.5}\text{Sr}_{0.5}\text{Cu}_{2.2}\text{Ti}_{1.8}\text{O}_{11-\delta}$	10.78 ± 0.02	0.00 ± 0.01	Air-quenched
Quintuple samples			
$\text{NdDyCaBa}_{1.5}\text{Sr}_{0.5}\text{Cu}_{2.2}\text{Ti}_{2.8}\text{O}_{14-\delta}$	13.83 ± 0.02	0.02 ± 0.01	Air-quenched
$\text{NdDyCaBa}_{1.5}\text{Sr}_{0.5}\text{Cu}_{2.2}\text{Ti}_{2.8}\text{O}_{14-\delta}$	13.81 ± 0.02	0.00 ± 0.01	Oxygen-annealed
$\text{NdDyCaBa}_{1.9}\text{Sr}_{0.1}\text{Cu}_{2.2}\text{Ti}_{2.8}\text{O}_{14-\delta}$	13.82 ± 0.02	0.02 ± 0.01	Air-quenched

improved electrical properties of these samples (see below). The $x = 0.5$ quadruple perovskite sample with the very small a and c lattice parameters has a high oxygen content and a low thermopower value, both indicative of enhanced hole content.

Electrical Characterization

A useful analysis method combining high-temperature thermopower and conductivity measurements, first presented by Jonker (37), was applied in this study. The technique consists of plotting thermopower versus the natural logarithm of conductivity, resulting in a characteristic “pear” shape (38). It is useful for interpreting electrical properties (i.e., carrier density, band gap, mobility, and density of states). The data are fitted with a two-band semiconductor model (34). The location and size of the pear, the region of the curve where the data fall, and the spread of the data as a function of oxygen partial pressure or chemical substitution provide a great deal of information about the defect chemistry and transport properties of a given material.

An important feature of the Jonker pear is that the sign of the thermopower is that of the majority carrier. Carrier concentration increases clockwise around the pear for holes and counterclockwise for electrons. There are two main regions on the pear. The low-conductivity (intrinsic) regime is where both electrons and holes contribute to the electrical properties and the thermopower changes rapidly with small changes in conductivity. The linear (extrinsic) region is on the high-conductivity side of the diagram, where a single carrier contributes to the conductivity and thermopower. The ideal slope of a given leg is $-k/e$ for p -type material and $+k/e$ for n -type material (k is Boltzmann’s constant and e is the unit of electronic charge). The size of the pear is determined by the band gap. The intercept of the extrinsic leg of the plot with the conductivity axis is called σ_{\max} and is related to the product of the density of states (DOS) and mobility (μ). A transition from intrinsic behavior to extrinsic behavior is observed when the copper–oxygen sheets of the insulating parent compounds are properly doped. The data of superconducting compounds fall toward the high-conductivity intercept, often exhibiting a deviation from $\pm k/e$ linearity, indicative of a transition from semiconducting to heavily doped metallic behavior. The thermopower threshold value for superconductivity is $\sim 45 \mu\text{V/K}$.

Jonker plots of $\text{NdDyBa}_{2-x}\text{Sr}_x\text{Cu}_{2+y}\text{Ti}_{2-y}\text{O}_{11-\delta}$ ($x = 0, 0.1, 0.3, 0.5$ and $y = 0, 0.2$) and $\text{NdDyCaBa}_{2-x}\text{Sr}_x\text{Cu}_{2+y}\text{Ti}_{3-y}\text{O}_{14-\delta}$ ($x = 0, 0.1, 0.5$ and $y = 0.2$) are shown in Figs. 5a–5c. A significant shift of the pear along the conductivity axis is observed as the result of B-site hole doping of the parent quadruple compound in Fig. 5a, implying that the density of states near the Fermi level and/or the carrier mobility is enhanced. The fact that data for the B-site doped system fall more toward the extrinsic leg of the plot com-

pared to that of the parent compound implies an increased hole content of the system. Figures 5b and 5c show that the data points for the quadruple system as well as those for the quintuple system shift toward the higher conductivity intercept (σ_{\max}) by substituting only 5% Sr for Ba. As the Sr level increases further to 25%, the plots shift in the reverse direction along the conductivity axis. The thermopower values do not change significantly upon Sr doping in either quadruple or quintuple systems.

There are interesting differences between the quadruple and quintuple system behaviors. The doping in quintuple perovskites seems to be ineffective, owing to the structural factors. The data points on Jonker plots of the quintuple samples fall more toward the intrinsic region of the pear compared to those on plots of the quadruple specimens, and they are less distributed along the curve. The narrower distribution in the Jonker plot of the quintuple perovskites, i.e., the smaller dependence of carrier concentration on oxygen partial pressure than in the quadruple systems, is thought to be due to the inherently compact structure of quintuple compounds as explained above. Quintuple-perovskite compounds have shorter bond lengths along both the a and c axes (evidenced by their structural refinement data). Their compact structure presumably makes oxygen refilling (either in vacant sites of the blocking layer or as oxygen interstitial defect species between the CuO_2 sheets) more difficult and yields this oxygen insensitivity.

An alternative explanation for the difference in the extent of data spread along the Jonker curve can be due to cationic intermixing among the A sites. A-cation intermixing may prove to be more severe in the NdDy quadruple systems than in the quintuple counterparts. The presence of larger Nd in the smaller Dy sites will expand the space between the Cu–O planes, making it easier to intercalate oxygen interstitials; hence a wider spread of data along the Jonker curve as observed in the quadruple system. A neutron diffraction study is now in progress to estimate the extent of cationic disorder in these systems.

Figure 6 shows the slow-cooling data of the NdDy quadruple systems. These data were collected from the samples under ambient pressure of oxygen cooling at 20°C/h rate from 800 to 400°C , and represent the dependence of the electrical properties on temperature. What is noticeable in the slow-cooling plot of $\text{NdDyBa}_{2-x}\text{Sr}_x\text{Cu}_{2.2}\text{Ti}_{1.8}\text{O}_{11-\delta}$ is the significant drop in thermopower of these samples as they cool, suggesting that the carrier concentration is increasing as the temperature decreases (while the DOS–mobility product remains roughly constant). Among the slow-cooling data, the $x = 0.5$ sample has the lowest thermopower, right on the borderline of superconductivity (approaching $45 \mu\text{V/K}$) (16). This sample displays the highest Cu oxidation state ($p = 0.12$ per copper) and the shortest Cu–O bond length ($\sim 1.94 \text{ \AA}$) according to TGA (Table 1) and X-ray diffraction (Fig. 4a), respectively. For both this and

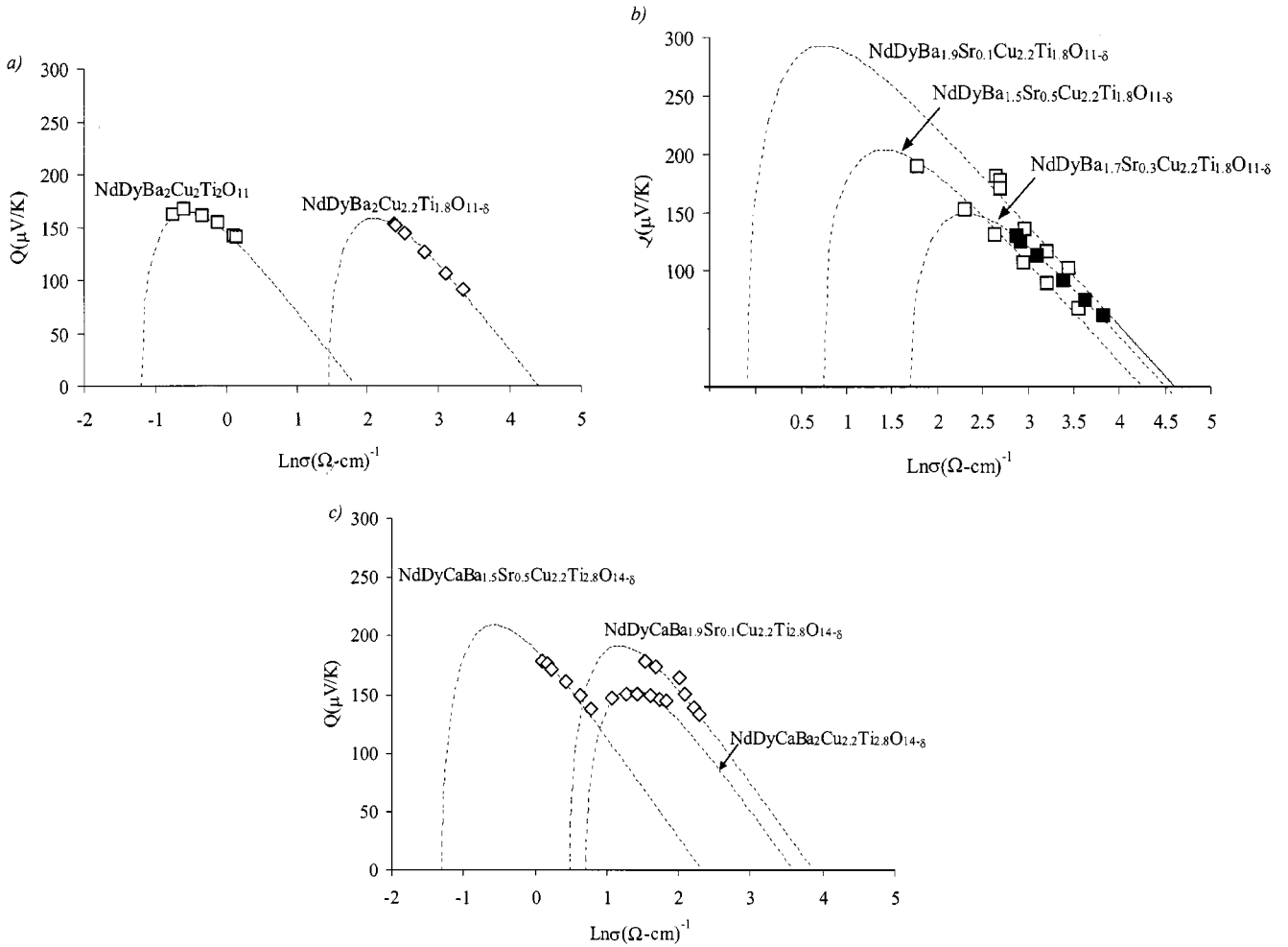


FIG. 5. Jonker pears fitted to the measured data for (a) the undoped quadruple parent compound at 750°C vs the B-site doped sample at 800°C , (b) Sr co-substituted quadruple perovskites at 750°C , and (c) Sr co-substituted quintuple perovskites at 800°C . Oxygen partial pressures increases clockwise around the pear at values of 10^{-5} , 10^{-4} , 10^{-3} , 10^{-2} , 10^{-1} , and 1 atm.

the $x = 0.1$ sample there is a noticeable deviation from linear behavior near 400°C . The straight lines in Fig. 6 represent the slope expected for an extrinsic semiconductor, and deviation toward higher conductivity values is consistent with a semiconductor-to-metal transition (11). The same deviation is observed in the Jonker plots of known high T_c layered cuprate superconductors. The two compounds that show the most deviation from semiconducting behavior in Fig. 6 ($x = 0.1$ and 0.5) also exhibit a metal-insulator transition in their low-temperature resistivity plots (Fig. 7).

A master plot of the high-temperature Seebeck coefficients (Q) of various known layered cuprate superconductors vs their hole concentration provides a useful means to evaluate the potential of new materials for superconductivity (Fig. 8a). The hole concentrations were calculated based on the oxygen content data in the literature (39–44). The Seebeck coefficients were measured under flowing oxygen at

$\sim 700^\circ\text{C}$ (45–50). A dashed line in Fig. 8a separates the data for nonsuperconducting (low hole content) and superconducting (high hole content) materials. Some data for quadruple perovskites from the present study fall to the right of the boundary in the superconducting regime (such as the $\text{NdDyBa}_{1.5}\text{Sr}_{0.5}\text{Cu}_{2.2}\text{Ti}_{1.8}\text{O}_{11-\delta}$ material) as shown in Fig. 8b. This indicates that carrier concentrations necessary for superconductivity have been achieved in these materials; nevertheless, they are not superconducting, as evidenced by low-temperature magnetic susceptibility and resistivity measurements.

There are several plausible reasons that the quadruple perovskites remain nonsuperconducting despite good high-temperature thermopower and conductivity results indicative of suitable doping (see Fig. 8b). First, it is conceivable that some mechanism of carrier trapping reduces the free hole content at lower temperatures. Attempts to measure carrier content on the most highly doped specimen by the

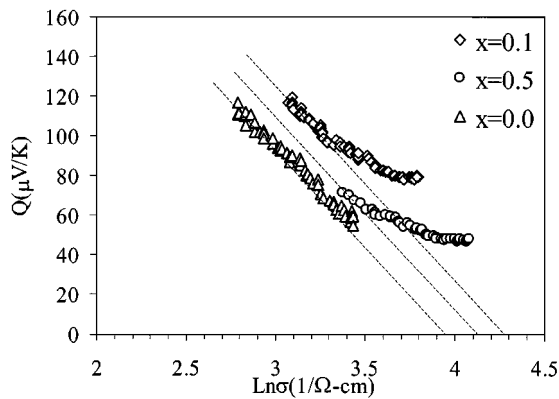


FIG. 6. Simultaneous thermopower–conductivity measurements on $\text{NdDyBa}_{2-x}\text{Sr}_x\text{Cu}_{2.2}\text{Ti}_{1.8}\text{O}_{11-\delta}$ quadruple systems, slow-cooled at a $20^\circ\text{C}/\text{h}$ rate from ≈ 800 to 400°C in flowing oxygen.

Hall effect at room temperature and below were inconclusive. Based on the specimen geometry and magnetic field employed (7400 G), we were able to estimate a lower limit for carrier content in these materials on the order of $10^{21}/\text{cm}^3$. This value is comparable to that of known superconductors and supports our contention that the carrier concentration of these materials has reached the level necessary for superconductivity. Another possibility is that oxygen interstitials are introduced, between Cu–O layers, owing to some measure of cation intermixing between the A' and A'' sites, which disrupts the structural integrity essential for superconductivity. Finally, the thickness and the nature of the blocking layer can affect the superconducting behavior of the layered cuprate perovskites. A thick blocking layer may prevent the necessary coupling between Cu–O layers,

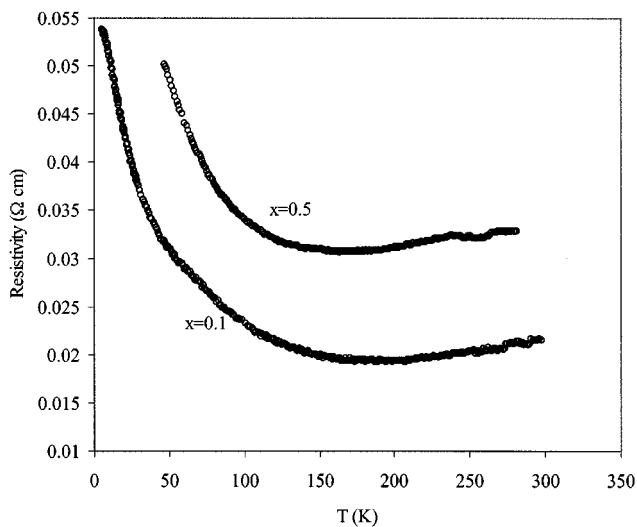


FIG. 7. The low-temperature resistivity plots for $\text{NdDyBa}_{2-x}\text{Sr}_x\text{Cu}_{2.2}\text{Ti}_{1.8}\text{O}_{11-\delta}$ ($x = 0.1$ and 0.5).

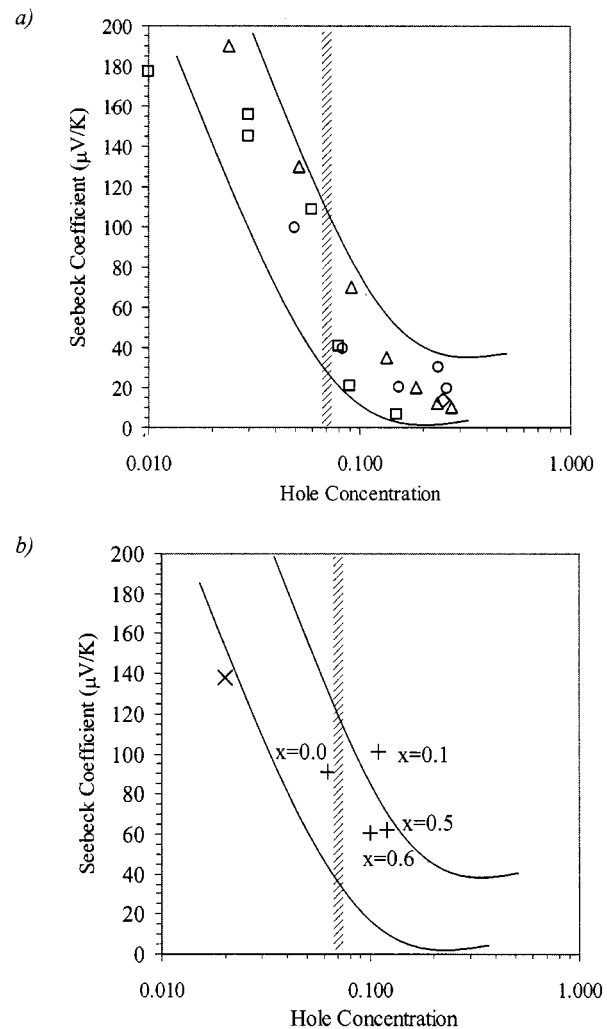


FIG. 8. Master plot of Seebeck coefficient–hole concentration for known superconductors. (a) Symbols correspond to cuprate materials of various doping levels (temperature $\sim 700^\circ\text{C}$): circles for $\text{La}_{2-x}\text{Sr}_x\text{CuO}_{4-\delta}$, triangles for $\text{La}_{2-x}\text{Ba}_x\text{CuO}_{4-\delta}$, squares for $\text{Bi}_{2.1}\text{Sr}_{1.9}(\text{Ca}_{1-x}\text{Y}_x)\text{Cu}_2\text{O}_{8+\delta}$, and diamonds for $\text{YBa}_2\text{Cu}_3\text{O}_8$. Specimens on the left-hand side of the dashed line do not superconduct whereas the ones on the right do. (b) Some data from the present study. Symbols used to show the compounds are + for $\text{NdDyBa}_{2-x}\text{Sr}_x\text{Cu}_{2.2}\text{Ti}_{1.8}\text{O}_{11-\delta}$ (the data for $x = 0.5$ and 0.6 fall in the superconducting region) and \times for $\text{NdDyCaBa}_{1.9}\text{Sr}_{0.1}\text{Cu}_{2.2}\text{Ti}_{2.8}\text{O}_{14-\delta}$.

thereby prohibiting superconductivity. The known layered cuprate superconductor with the largest blocking layer is $\text{Pb}_2\text{Sr}_2\text{YCu}_3\text{O}_8$ (c axis = 15.730 \AA) (51), which is comparable to the blocking layer of the quadruple perovskites in the present study (e.g., $\text{NdDyBa}_{1.5}\text{Sr}_{0.5}\text{Cu}_{2.2}\text{Ti}_{1.8}\text{O}_{11-\delta}$, c axis = 15.649 \AA). This comparison suggests that not only the thickness but also the nature of the blocking layer plays an important role in superconducting behavior of these materials. The plumbate blocking layer in $\text{Pb}_2\text{Sr}_2\text{YCu}_3\text{O}_8$ has a strong metallic nature and may facilitate coupling

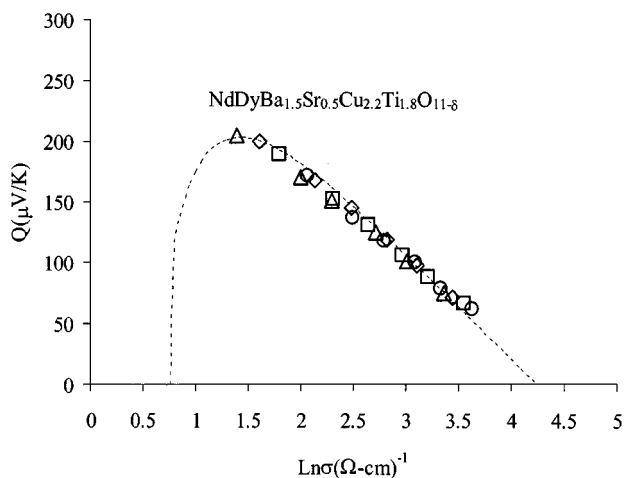


FIG. 9. Jonker pear fitted to the measured data for the $\text{NdDyBa}_{1.5}\text{Sr}_{0.5}\text{Cu}_{2.2}\text{Ti}_{1.8}\text{O}_{11-\delta}$ quadruple sample at different temperatures. Oxygen partial pressure increases clockwise around the pear at values of 10^{-5} , 10^{-4} , 10^{-3} , 10^{-2} , 10^{-1} , and 1 atm. Symbols correspond to different temperatures: circles for 650°C , triangles for 700°C , squares for 750°C , and diamonds for 800°C .

between Cu–O layers, thereby improving the electronic behavior of the system. However, in $\text{NdDyBa}_{1.5}\text{Sr}_{0.5}\text{Cu}_{2.2}\text{Ti}_{1.8}\text{O}_{11-\delta}$ the rather insulating nature of the titanate blocking layer, along with its large thickness, may prevent coupling and inhibit superconductivity.

One interesting observation is the apparent absence of band gap variation with temperature for the quadruple perovskites, as observed in Fig. 9. Notice that the data for all four temperatures lie on a single Jonker pear. This is in sharp contrast to all known layered cuprate superconductors (38), where the size of the pear (and band gap) decreases with increasing temperature. This may suggest a fundamental difference between the electronic structures of the quadruple perovskites in the present study and the superconducting perovskites.

As discussed previously, the σ_{max} in Jonker plots increases with Sr doping up to $x = 0.1$ and then decreases (see Figs. 5b and 5c). The same trend of σ_{max} is observed in slow-cooling plots; the σ_{max} intercept moves toward higher conductivity up to $x = 0.1$ and then decreases with further Sr substitution ($x = 0.5$). Since the σ_{max} intercept in Jonker plots is related to the $\text{DOS}-\mu$ product, the variations in σ_{max} imply a change in carrier mobility, density of states, or both. Hall measurements under a higher magnetic field or alternatively on thin films should be able to resolve this issue.

CONCLUSION

There is a complex interplay between the electrical properties of quadruple- and quintuple-layered cuprates and

their defect chemistry, solid solution behavior, and oxygen intercalation. Extensive substitutions are possible, i.e., $0 \leq x \leq 0.6$ and $0 \leq y \leq 0.2$ in the $\text{NdDyBa}_{2-x}\text{Sr}_x\text{Cu}_{2+y}\text{Ti}_{2-y}\text{O}_{11-\delta}$ system and $0.0 \leq x \leq 0.5$ and $0.0 \leq y \leq 0.2$ in the $\text{NdDyCaBa}_{2-x}\text{Sr}_x\text{Cu}_{2+y}\text{Ti}_{3-y}\text{O}_{14-\delta}$ system. Thermogravimetry results show that, for the quadruple samples of $\text{NdDyBa}_{2-x}\text{Sr}_x\text{Cu}_{2.2}\text{Ti}_{1.8}\text{O}_{11-\delta}$, Sr substitution for Ba allows refilling of oxygen vacancies introduced during ionic compensation of the aliovalent dopant, $[\text{Cu}_{\text{Ti}}]$. Sr occupation in Ba sites presumably provides more space around the oxygen vacancies so that refilling those vacancies becomes energetically favorable. Oxygen contents as high as 10.92–10.93 and thermopower values as low as $45 \mu\text{V/K}$ were obtained for the $x = 0.1$ – 0.5 compounds, corresponding to partial electronic compensation ($p \sim 0.1$ per copper).

Slow-cooling Q – $\ln \sigma$ data for quadruple $\text{NdDyBa}_{2-x}\text{Sr}_x\text{Cu}_{2.2}\text{Ti}_{1.8}\text{O}_{11-\delta}$ materials ($x = 0.1, 0.5$) show an improvement in electrical properties with Sr substituted for Ba. Furthermore, these data show a deviation from two-band semiconductor behavior with decreasing temperature. This is consistent with the semiconductor-to-metallic transition that has been confirmed by low-temperature resistivity measurements. The σ_{max} intercept increases up to $x = 0.1$; thereafter, it decreases.

The Sr-substituted NdDy quadruple system has shown the most suitable structural aspects for doping so that vacant oxygen sites in the blocking layer (introduced as a compensation during copper substitution) can be filled more effectively than those in other quadruple or quintuple compounds studied. On a master plot of thermopower vs hole concentration of known cuprate compounds, selected NdDy quadruple specimens fall in the superconducting region, implying that they have the necessary carrier concentration for superconductivity. Their failure to superconduct suggests that other structural factors, e.g., cationic disordering between A' and A'' sites (permitting oxygen interstitials between Cu–O layers), an overly large blocking layer thickness, and/or an insulating rather than metallic blocking layer (preventing coupling between Cu–O layers) prohibits superconductivity.

ACKNOWLEDGMENTS

This work was initiated under support from the National Science Foundation (DMR 91-20000) through the Science and Technology Center for Superconductivity and is currently supported by the U.S. Department of Energy under Grant DE-FGO2-84ER45097. The authors are grateful to M. Rocci-Lane and C. R. Kannewurf for their help with Hall effect measurements.

REFERENCES

1. M. T. Anderson, K. R. Poeppelmeier, J. P. Zhang, H. J. Fan, and L. D. Marks, *Chem. Mater.* **4**, 1305–1313 (1992).

2. A. Gormezano and M. T. Weller, *J. Mater. Chem.* **3**, 771–772 (1993).
3. A. Gormezano and M. T. Weller, *J. Mater. Chem.* **3**, 979 (1993).
4. K. B. Greenwood, M. T. Anderson, K. R. Poeppelmeier, D. L. Novikov, A. J. Freeman, B. Dabrowski, S. A. Gramsch, and J. K. Burdett, *Physica C* **235–240**, 349–350 (1994).
5. M. H. Kane, M. S. dissertation, Northwestern University, 1997.
6. K. D. Otszchi, K. R. Poeppelmeier, P. A. Salvador, T. O. Mason, H. Zhang, and L. D. Marks, *J. Am. Chem. Soc.* **118**, 8951–8952 (1996).
7. K. D. Otszchi, K. R. Poeppelmeier, P. A. Salvador, T. O. Mason, W. Sinkler, H. Zhang, and L. D. Marks, *Physica C* **282–287**, 837–838 (1997).
8. P. A. Salvador, T. O. Mason, K. Otszchi, K. B. Greenwood, K. R. Poeppelmeier, and B. Dabrowski, *J. Am. Chem. Soc.* **119**, 3756–3764 (1997).
9. M. R. Palacin, A. Fuertes, N. Casan-Paster, and P. Gomez-Romero, *Adv. Mater.* **6**, 54–57 (1994).
10. M. R. Palacin, A. Fuertes, N. Casan-Pastor, and P. Gomez-Romero, *J. Solid State Chem.* **119**, 224–236 (1995).
11. M. R. Palacin, N. Casan-Pastor, G. Kramer, M. Jansen, and P. Gomez-Romero, *Physica C* **261**, 71–80 (1996).
12. M. R. Palacin, F. Krumeich, and P. Gomez-Romero, *Solid State Ionic* **101–103**, 1079–1085 (1997).
13. M. R. Palacin, N. Casan-Pastor, and P. Gomez-Romero, *J. Solid State Chem.* **138**, 141–148 (1998).
14. M. H. Kane, N. Mansourian-Hadavi, T. O. Mason, W. Sinkler, L. D. Marks, K. D. Otszchi, D. Ko, and K. R. Poeppelmeier, *J. Solid State Chem.* **148**, 3–15 (1999).
15. D. L. Novikov, A. J. Freeman, and K. R. Poeppelmeier, *Phys. Rev. B* **53**, 9448–9452 (1996).
16. P. A. Salvador, Ph.D. dissertation, Northwestern University, 1997.
17. K. B. Greenwood, G. M. Sarjeant, K. R. Poeppelmeier, P. A. Salvador, T. O. Mason, B. Dabrowski, K. Rogacki, and Z. Chen, *Chem. Mater.* **7**, 1355–1360 (1995).
18. J. B. Goodenough, *Supercond. Sci. Technol.* **3**, 26 (1990).
19. J. B. Goodenough and A. Manthiram, *J. Solid State Chem.* **88**, 115–139 (1990).
20. H. Zhang and H. Sato, *Phys. Rev. Lett.* **70**, 1697–1699 (1993).
21. J. Gopalakrishnan, R. Vijayaraghavan, R. Nagarajan, and C. Shivakumara, *J. Solid State Chem.* **93**, 272–275 (1991).
22. J.-M. Tarascon, P. Barboux, G. W. Hull, R. Ramesh, L. H. Greene, M. Giroud, M. S. Hegde, and W. R. McKinnon, *Phys. Rev.* **39**, 4316–4326 (1989).
23. D. M. D. Leeuw, W. A. Groen, J. C. Jol, H. B. Brom, and H. W. Zandbergen, *Physica C* **166**, 349–356 (1990).
24. J. B. Torrance, Y. Tokura, A. I. Nazzari, A. Bezinge, T. C. Huang, and S. S. P. Parkin, *Phys. Rev. Lett.* **61**, 1127–1130 (1988).
25. J. L. Tallon, *Physica C* **176**, 547–550 (1991).
26. S. Nakajima, M. Kikuchi, Y. Syone, K. Nagase, T. Oku, N. Kabayashi, D. Shindo, and K. Hirage, *Physica C* **170** (1990).
27. Y. Tokura, H. Takagi, and S. Uchida, *Nature* **337**, 345 (1989).
28. B. S. Hong Ph.D. dissertation, Northwestern University, 1994.
29. D. L. J. Hong and D. M. Smyth, *J. Phys. Chem. Solids* **55**, 1405–1413 (1994).
30. M. J. Pack, A. Gormezano, and M. T. Waller, *Chem. Mater.* **9**, 1547–1553 (1997).
31. P. Gomez-Romero, M. R. Palacin, C. R. Michel, and N. Casan-Pastor, *Solid State Ionics* **101–103**, 411–415 (1997).
32. A. LeBail, H. Duroy, and J. L. Fourquet, *Mater. Res. Bull.* **23**, 447–452 (1988).
33. A. C. Larson and R. B. V. Dreele, National Laboratory Neutron Scattering Center, Los Alamos, NM, 1985.
34. P. A. Salvador, L. Shen, T. O. Mason, K. B. Greenwood, and K. R. Poeppelmeier, *J. Solid State Chem.* **119**, 80–89 (1995).
35. A. Trestman-Matts, S. E. Dorris, and T. O. Mason, *J. Am. Ceram. Soc.* **66**, 589–592 (1983).
36. D. S. McLachlan, M. Blaszkiewicz, and R. E. Newnham, *J. Am. Ceram. Soc.* **73**, 2186–2203 (1990).
37. G. H. Jonker, *Philips Res. Rep.* **23**, 131–138 (1968).
38. M. Su, C. E. Elsbernd, and T. O. Mason, *J. Am. Ceram. Soc.* **73**, 415–419 (1990).
39. L. Shen, P. A. Salvador, and T. O. Mason, *J. Am. Ceram. Soc.* **77**, 81–88 (1994).
40. E. J. Opila and H. L. Tuller, *J. Am. Ceram. Soc.* **77**, 2727–2737 (1994).
41. E. Takayama-Muromachi and D. E. Rice, *Physica C* **177**, 195–206 (1991).
42. C. Rial, E. Moran, M. A. Alario-Franco, U. Amador, J. L. Martinez, J. Rodrigues-Carvajal, and N. H. Andersen, *Physica C* **297**, 277–293 (1998).
43. J. D. Jorgensen, *Phys. Today* 34–40 (June 1991).
44. W. A. Groen, D. M. d. Leeuw, and L. F. Feiner, *Physica C* **165**, 55–61 (1990).
45. D. J. L. Hong and D. M. Smyth, *J. Solid State Chem.* **102**, 250–260 (1993).
46. M. Y. Su, E. A. Cooper, C. E. Elsbernd, and T. O. Mason, *J. Am. Ceram. Soc.* **73**, 3453–3456 (1990).
47. L. Shen, P. A. Salvador, and T. O. Mason, *J. Phys. Chem. Solids* **57**, 1311–1319 (1996).
48. T. O. Mason, Ed., “Defect Chemistry of High T_c Superconducting Cuprates,” Vols. 66&67. Trans. Tech. Publications, Zurich, 1992.
49. B.-S. Hong and T. O. Mason, *J. Mater. Res.* **6**, 2054–2058 (1991).
50. B. Hong and T. O. Mason, *J. Am. Ceram. Soc.* **76**, 635–640 (1993).
51. R. J. Cava, M. Marezio, J. J. Krajewski, W. F. Peck, Jr., A. Santoro, and F. Beech, *Physica C* **157**, 272 (1989).